remote sensing

MDPI

Communication

Adaptive Robust Radar Target Detector Based on Gradient Test

Zeyu Wang [1,*], Jun Liu [2], Hongmeng Chen [3] and Wei Yang [3]

[1] State Key Laboratory of Networking and Switching Technology, Beijing University of Posts and Telecommunications, Beijing 100876, China
[2] Department of Electronic Engineering and Information Science, University of Science and Technology of China, Hefei 230027, China
[3] Beijing Institute of Radio Measurement, Beijing 100854, China
* Correspondence: zeyuwang@bupt.edu.cn

Abstract: The exact knowledge of the signal steering vector is not always known, which may result in detection performance degradation when a signal mismatch occurs. In this paper, we discuss the problem of designing a robust radar target detector in the background of Gaussian noise whose covariance matrix is unknown. To improve robustness to mismatched signals, a random perturbation that follows the complex normal distribution is added under the alternative hypothesis. Since traditional detectors that divide complex parameters into real parts and imaginary parts are sometimes difficult to obtain, a new robust, complex parameter gradient test is derived directly from the complex data. Moreover, the CFAR property of the new detector is proven. The performance assessment indicates that the gradient detector exhibits suitable robustness to the mismatched signals.

Keywords: radar target; adaptive detection; gradient test; signal mismatch

Citation: Wang, Z.; Liu, J.; Chen, H.; Yang, W. Adaptive Robust Radar Target Detector Based on Gradient Test. *Remote Sens.* **2022**, *14*, 5236. https://doi.org/10.3390/rs14205236

Academic Editor: Gerardo Di Martino

Received: 28 August 2022
Accepted: 18 October 2022
Published: 20 October 2022

1. Introduction

Adaptive detection algorithms have gained increasing interest among scholars in the fields of radar, sonar, and communications in recent decades due to their flexible design criteria. In a seminal paper, Kelly [1] used statistical hypothesis testing techniques to address the signal detection problem and derived a generalized likelihood ratio test (GLRT) to decide whether targets exist or not. Subsequently, Robey et al. [2] first utilized the GLRT test statistic using only the data under test and then plugged the sample covariance matrix (CM) into the test statistic to obtain the adaptive matched filter (AMF). De Maio [3] proved that the Wald test and the AMF coincide when detecting signals with known steering vectors and unknown amplitudes. When the target signal lies in a subspace of dimension not less than 1, Kraut et al. [4] proposed adaptive subspace detectors using no prior knowledge of noise CM. Later, the Rao test, which is more selective to sidelobe signals than Kelly's GLRT, was proposed in [5]. Adaptive target detection problems in other scenarios, such as training-limited environments and nonhomogeneous clutter environments, have been studied in [6–11].

Most of the adaptive detectors discussed above assume that the signal signature is completely known. However, when beam pointing errors, array calibration errors, or sidelobe signals exist, the nominal steering vector is no longer equal to the actual one [12]. Adaptive detectors can be categorized as mismatch selective detectors and mismatch robust detectors based on their sensitivity to mismatched signals. Robust detectors can still provide high detection probabilities in the case of signal mismatch, while selective detectors achieve stronger rejection capabilities of mismatched signals. To enhance sensitivity, a fictitious interference that is orthogonal to the presumed target signals in the quasi-whitened space or the truly whitened observation space was added under the null hypothesis to design an adaptive beamformer orthogonal rejection test [13] and its modified algorithm [14]. Some other selective detectors were designed in [15,16].

Radars in scan mode prefer a detector that is more robust to the mismatched signals. To improve robustness, three GLRT-based adaptive detectors [17] were proposed by assuming that the real parts and imaginary parts of the target steering vector belong to the union of two convex cones. The three detectors perform better than Kelly's GLRT, AMF, and adaptive beamformer orthogonal rejection test in mismatched signal cases, respectively. In [18], three adaptive robust detectors for MIMO radar were proposed by adopting a subspace model to represent the transmit signals or receive signals. Considering that the improper choice of signal subspace may result in certain performance loss, Besson [19] assumed that the angle between the presumed signal and actual signal is bounded and derived GLRT detector by solving a semidefinite programming problem. The proposed GLRT is more robust but suffers certain matched performance loss compared to the generalized adaptive subspace detector. In [20], subspace constraint, the adaptive beamformer orthogonal rejection test, and conic uncertainty set constraint techniques were combined to derive the adaptive polarimetric radar detector. More recently, target echoes were modeled as the sum of a random signal, noise, and target signal to increase the plausibility of the alternative hypothesis in [21]. The resulting detectors can achieve increased robustness and similar matched detection performance with Kelly's GLRT.

Since a uniformly most powerful (UMP) test is lacking for the problem of detecting signals with known steering vectors and unknown amplitudes [5] in Gaussian noise, it is necessary to derive new adaptive detectors according to other test criteria and evaluate the detection performance [22]. The gradient test is a commonly used test criterion other than GLRT, Rao, and Wald tests [23]. This paper discusses adaptive radar target detection problems when a signal mismatch occurs. A complex parameter gradient test is resorted to proposing a new adaptive detector. To improve robustness, we modify the alternative hypothesis by introducing a random perturbation that follows a complex normal distribution with the CM proportional to the noise CM. Moreover, the test statistic is derived directly based on complex parameters instead of dividing them into real and imaginary parts. The constant false alarm rate (CFAR) property of the new detector is proved with respect to the noise CM. The performance evaluation shows that the new gradient detector achieves suitable detection performance in mismatched signal scenarios.

We organize the remainder of the paper as follows. Section 2 gives the problem formulation of the problem at hand. The design of the adaptive robust gradient detector is shown in Section 3. Matched and mismatched detection performance analysis is given in Section 4. In Section 5, we conclude this paper.

2. Problem Formulation

The received radar echoes are denoted by $\boldsymbol{y}_0 \in \mathbb{C}^{N\times 1}$, where N is the number of coherent pulses or the product of pulse numbers and antenna array elements [21,24]. We formulate the problem of target detection as a binary hypothesis test. Under the alternative hypothesis, the echoes include the noise $\boldsymbol{n}_0$ and useful target signal $\boldsymbol{s} = \alpha \boldsymbol{t}$. Under the null hypothesis, the echoes include only the noise $\boldsymbol{n}_0$. Here, $\boldsymbol{n}_0 \in \mathbb{C}^{N\times 1}$ follows a circularly symmetric complex normal (CSCN) distribution with zero mean, and CM $\boldsymbol{R}$, α denotes the target amplitude, $\boldsymbol{t} \in \mathbb{C}^{N\times 1}$ is the steering vector of the target. A random component $\boldsymbol{\omega}$ is added under the alternative hypothesis to improve the robustness of the mismatched signals. Then, the detection problem is equivalent to deciding which of the two hypotheses holds:

$$\begin{cases} H_0 : \begin{cases} \boldsymbol{y}_0 = \boldsymbol{n}_0, \\ \boldsymbol{y}_k = \boldsymbol{n}_k, k = 1, \ldots, K \end{cases} \\ H_1 : \begin{cases} \boldsymbol{y}_0 = \alpha \boldsymbol{t} + \boldsymbol{\omega} + \boldsymbol{n}_0, \\ \boldsymbol{y}_k = \boldsymbol{n}_k, k = 1, \ldots, K \end{cases} \end{cases} \tag{1}$$

where $\boldsymbol{y}_0$ are data under test or primary data, $\boldsymbol{Y}_k = [\boldsymbol{y}_1, \ldots \boldsymbol{y}_k, \ldots, \boldsymbol{y}_K], k = 1, \ldots, K$ are training data that are independent and identically distributed (i.i.d.) with the noise $\boldsymbol{n}_0$ in the primary data. The random perturbation $\boldsymbol{\omega}$ obeys zero mean CSCN distribution with CM $\delta \boldsymbol{R}$.

Then, the distributions of the received data under the two hypotheses are

$$\begin{cases} H_0: \begin{cases} \boldsymbol{y}_0 \sim CN(\boldsymbol{0}, \boldsymbol{R}), \\ \boldsymbol{y}_k \sim CN(\boldsymbol{0}, \boldsymbol{R}), k = 1, \ldots, K \end{cases} \\ H_1: \begin{cases} \boldsymbol{y}_0 \sim CN(\alpha \boldsymbol{t}, (1+\delta)\boldsymbol{R}), \\ \boldsymbol{y}_k \sim CN(\boldsymbol{0}, \boldsymbol{R}), k = 1, \ldots, K \end{cases} \end{cases} \tag{2}$$

where $CN(\cdot)$ denotes the CSCN distribution, δ is a real constant greater than 0.

According to the distribution of the received data, we calculate the joint probability density function (PDF) of the training data $\boldsymbol{Y}_k$ and the primary data $\boldsymbol{y}_0$ under H_ι as

$$f_\iota = \frac{1}{\pi^{N(1+K)}(1+\delta)^N |\boldsymbol{R}|^{K+1}} \exp\left\{ -\mathrm{tr}\left[\boldsymbol{R}^{-1} \left(\boldsymbol{S} + \frac{1}{(1+\iota\delta)} (\boldsymbol{y}_0 - \iota\alpha\boldsymbol{t})(\boldsymbol{y}_0 - \iota\alpha\boldsymbol{t})^H \right) \right] \right\} \tag{3}$$

where $\iota = 0, 1$, $\boldsymbol{S} = \sum_{k=1}^{K} \boldsymbol{y}_k \boldsymbol{y}_k^H$, $|\cdot|$ denotes determinant, $(\cdot)^H$ denotes conjugate transpose, $\mathrm{tr}(\cdot)$ denotes trace.

3. Design of Adaptive Robust Detector

For brevity, we set $\boldsymbol{\Theta}_r = \left[\alpha^T, \alpha^H, \delta\right]^T$, $\boldsymbol{\Theta}_s = \mathrm{vec}(\boldsymbol{R})$, $\boldsymbol{\Theta} = \left[\boldsymbol{\Theta}_r^T, \boldsymbol{\Theta}_s^T\right]^T$, where $\boldsymbol{\Theta}$ is an $\left(N^2+3\right)$-dimensional column vector. We resort to a one-step complex parameter gradient test to design an adaptive detector.

3.1. Adaptive Robust Gradient Detector

The complex parameter gradient test is

$$T_{Gradient} = \left. \frac{\partial \ln f_1}{\partial \boldsymbol{\Theta}_r^T} \right|_{\boldsymbol{\Theta} = \hat{\boldsymbol{\Theta}}_0} \left(\hat{\boldsymbol{\Theta}}_{r1} - \boldsymbol{\Theta}_{r0} \right) \underset{H_0}{\overset{H_1}{\gtrless}} \eta \tag{4}$$

where $\hat{\boldsymbol{\Theta}}_0$ is the maximum likelihood estimate (MLE) of $\boldsymbol{\Theta}$ under H_0, $\boldsymbol{\Theta}_{r0}$ is the value of $\boldsymbol{\Theta}_r$ under H_0, $\hat{\boldsymbol{\Theta}}_{r1}$ is the MLE of $\boldsymbol{\Theta}_r$ under H_1, $(\cdot)^T$ is transpose, $\ln(\cdot)$ denotes the logarithm, η denotes the detection threshold.

We substitute $\boldsymbol{\Theta}_r$ into the test statistic (4) and get

$$\frac{\partial \ln f_1}{\partial \boldsymbol{\Theta}_r^T} = \left(\frac{\partial \ln f_1}{\partial \boldsymbol{\Theta}_r^*} \right)^H = \begin{bmatrix} \frac{\partial \ln f_1}{\partial \alpha^*} \\ \frac{\partial \ln f_1}{\partial \alpha} \\ \frac{\partial \ln f_1}{\partial \delta} \end{bmatrix}^H \tag{5}$$

According to the differential theory of complex matrices, we take the partial differential of the logarithm of the joint PDF (3) under H_1 with respect to $\boldsymbol{\Theta}_r^*$ and have the following results

$$\frac{\partial \ln f_1}{\partial \alpha^*} = \frac{1}{1+\delta} \left(\boldsymbol{t}^H \boldsymbol{R}^{-1} \boldsymbol{y}_0 - \alpha \boldsymbol{t}^H \boldsymbol{R}^{-1} \boldsymbol{t} \right) \tag{6}$$

$$\frac{\partial \ln f_1}{\partial \alpha} = \frac{1}{1+\delta} \left(\boldsymbol{y}_0^H \boldsymbol{R}^{-1} \boldsymbol{t} - \alpha^H \boldsymbol{t}^H \boldsymbol{R}^{-1} \boldsymbol{t} \right)^T \tag{7}$$

$$\frac{\partial \ln f_1}{\partial \delta} = -\frac{N}{1+\delta} + \frac{1}{(1+\delta)^2} \left[(\boldsymbol{y}_0 - \alpha\boldsymbol{t})^H \boldsymbol{R}^{-1} (\boldsymbol{y}_0 - \alpha\boldsymbol{t}) \right] \tag{8}$$

From the test statistic (4), it can be seen that the MLE of $\boldsymbol{\Theta}$ under H_0 and the MLE of $\boldsymbol{\Theta}_r$ under H_1 are also needed. After some calculation, we obtain

$$d_{\boldsymbol{R}} \ln f_1 = -(K+1)\mathrm{tr}\left(\boldsymbol{R}^{-1} d\boldsymbol{R} \right) + \mathrm{tr}\left\{ \left[\boldsymbol{S} + (\boldsymbol{y}_0 - \alpha\boldsymbol{t})(\boldsymbol{y}_0 - \alpha\boldsymbol{t})^H / (1+\delta) \right] \boldsymbol{R}^{-1} d\boldsymbol{R} \boldsymbol{R}^{-1} \right\} \tag{9}$$

$$\hat{\boldsymbol{R}}_1 = \left[\boldsymbol{S} + \frac{1}{(1+\delta)}(\boldsymbol{y}_0 - \alpha\boldsymbol{t})(\boldsymbol{y}_0 - \alpha\boldsymbol{t})^H\right]/(K+1) \tag{10}$$

$$\hat{\boldsymbol{R}}_0 = \left(\boldsymbol{S} + \boldsymbol{y}_0\boldsymbol{y}_0^H\right)/(K+1) \tag{11}$$

$$\hat{\boldsymbol{\Theta}}_0 = \left[\boldsymbol{0}_{1\times 3}, \mathrm{vec}^T\left(\hat{\boldsymbol{R}}_0\right)\right]^T \tag{12}$$

where $\hat{\boldsymbol{R}}_0$ and $\hat{\boldsymbol{R}}_1$ are MLEs of $\boldsymbol{R}$ under H_0 and H_1 given α and δ. We can then obtain MLE of α given δ after substituting $\hat{\boldsymbol{R}}_1$ into the joint PDF (3)

$$\begin{aligned}\hat{\alpha} &= \underset{\alpha}{\mathrm{argmin}}\left|\boldsymbol{S} + (\boldsymbol{y}_0 - \alpha\boldsymbol{t})(\boldsymbol{y}_0 - \alpha\boldsymbol{t})^H/(1+\delta)\right| \\ &= \underset{\alpha}{\mathrm{argmin}}(1+\delta)^{-1}|\boldsymbol{S}|\left[(1+\delta) + (\boldsymbol{y}_0 - \alpha\boldsymbol{t})^H\boldsymbol{S}^{-1}(\boldsymbol{y}_0 - \alpha\boldsymbol{t})\right] \\ &= \frac{\boldsymbol{t}^H\boldsymbol{S}^{-1}\boldsymbol{y}_0}{\boldsymbol{t}^H\boldsymbol{S}^{-1}\boldsymbol{t}}\end{aligned} \tag{13}$$

We substitute $\hat{\alpha}$ and $\hat{\boldsymbol{R}}_1$ into joint PDF f_1 and find that the MLE of δ can be calculated by minimizing $(1+\delta)^{\frac{N}{K+1}}\left|\boldsymbol{S} + \frac{1}{(1+\delta)}(\boldsymbol{y}_0 - \hat{\alpha}\boldsymbol{t})(\boldsymbol{y}_0 - \hat{\alpha}\boldsymbol{t})^H\right|$ with respect to δ. Then, according to the properties of the determinant, we have the MLE of δ [21]

$$\begin{aligned}&\min_{\delta}(1+\delta)^{\frac{N}{K+1}}\left|\boldsymbol{S} + \tfrac{1}{(1+\delta)}(\boldsymbol{y}_0 - \hat{\alpha}\boldsymbol{t})(\boldsymbol{y}_0 - \hat{\alpha}\boldsymbol{t})^H\right| \\ &= \min_{\delta}|\boldsymbol{S}|(1+\delta)^{\frac{N}{K+1}-1}\left[1 + \delta + \widetilde{\boldsymbol{y}}_0^H\widetilde{\boldsymbol{y}}_0 - \widetilde{\boldsymbol{y}}_0^H\widetilde{\boldsymbol{t}}\left(\widetilde{\boldsymbol{t}}^H\widetilde{\boldsymbol{t}}\right)^{-1}\widetilde{\boldsymbol{t}}^H\widetilde{\boldsymbol{y}}_0\right]\end{aligned} \tag{14}$$

$$\hat{\delta} = \begin{cases} (\zeta-1)T - 1, (\zeta-1)T - 1 > 0 \\ 0, else \end{cases} \tag{15}$$

where $T = \widetilde{\boldsymbol{y}}_0^H\boldsymbol{P}_{\widetilde{\boldsymbol{t}}}^{\perp}\widetilde{\boldsymbol{y}}_0$, $\widetilde{\boldsymbol{y}}_0 = \boldsymbol{S}^{-\frac{1}{2}}\boldsymbol{y}_0$, $\widetilde{\boldsymbol{t}} = \boldsymbol{S}^{-\frac{1}{2}}\boldsymbol{t}$, $\boldsymbol{P}_{\widetilde{\boldsymbol{t}}}^{\perp} = \boldsymbol{I}_N - \widetilde{\boldsymbol{t}}\left(\widetilde{\boldsymbol{t}}^H\widetilde{\boldsymbol{t}}\right)^{-1}\widetilde{\boldsymbol{t}}^H$, $\zeta = \frac{K+1}{N}$.

The adaptive complex parameter gradient detector can be obtained by plugging (6)–(15) into (4) and simplifying the result:

$$T_{Gradient} = 2\mathrm{Re}\left(\frac{\boldsymbol{y}_0^H\hat{\boldsymbol{R}}_0^{-1}\boldsymbol{t}\boldsymbol{t}^H\boldsymbol{S}^{-1}\boldsymbol{y}_0}{\boldsymbol{t}^H\boldsymbol{S}^{-1}\boldsymbol{t}}\right) + \hat{\delta}\left[\mathrm{tr}\left(\boldsymbol{y}_0^H\hat{\boldsymbol{R}}_0^{-1}\boldsymbol{y}_0\right) - N\right] \underset{H_0}{\overset{H_1}{\gtrless}} \eta \tag{16}$$

3.2. CFAR Property Proof of the Gradient Detector

The test statistic of the gradient detector (16) is a function of $\frac{\boldsymbol{y}_0^H\hat{\boldsymbol{R}}_0^{-1}\boldsymbol{t}\boldsymbol{t}^H\boldsymbol{S}^{-1}\boldsymbol{y}_0}{\boldsymbol{t}^H\boldsymbol{S}^{-1}\boldsymbol{t}}$, $\boldsymbol{y}_0^H\hat{\boldsymbol{R}}_0^{-1}\boldsymbol{y}_0$, and $T = \widetilde{\boldsymbol{y}}_0^H\boldsymbol{P}_{\widetilde{\boldsymbol{t}}}^{\perp}\widetilde{\boldsymbol{y}}_0$. To prove the CFAR property of the gradient detector, we need only prove that the three expressions are independent of $\boldsymbol{R}$. According to the properties of the inverse matrix [25], we obtain

$$\begin{aligned}\hat{\boldsymbol{R}}_0^{-1} &= \left[\left(\boldsymbol{S} + \boldsymbol{y}_0\boldsymbol{y}_0^H\right)/(K+1)\right]^{-1} \\ &= (K+1)\left[\boldsymbol{S}^{-1} - \boldsymbol{S}^{-1}\boldsymbol{y}_0\left(1 + \boldsymbol{y}_0^H\boldsymbol{S}^{-1}\boldsymbol{y}_0\right)^{-1}\boldsymbol{y}_0^H\boldsymbol{S}^{-1}\right]\end{aligned} \tag{17}$$

Then, the three expressions can be simplified as

$$\begin{aligned}&\frac{\boldsymbol{y}_0^H\hat{\boldsymbol{R}}_0^{-1}\boldsymbol{t}\boldsymbol{t}^H\boldsymbol{S}^{-1}\boldsymbol{y}_0}{\boldsymbol{t}^H\boldsymbol{S}^{-1}\boldsymbol{t}} \\ &= (K+1)\left[1 - \boldsymbol{y}_0^H\boldsymbol{S}^{-1}\boldsymbol{y}_0\left(1 + \boldsymbol{y}_0^H\boldsymbol{S}^{-1}\boldsymbol{y}_0\right)^{-1}\right]\boldsymbol{y}_0^H\boldsymbol{S}^{-1}\boldsymbol{t}\boldsymbol{t}^H\boldsymbol{S}^{-1}\boldsymbol{y}_0\left(\boldsymbol{t}^H\boldsymbol{S}^{-1}\boldsymbol{t}\right)^{-1} \\ &= (K+1)\frac{\boldsymbol{y}_0^H\boldsymbol{S}^{-1}\boldsymbol{t}\boldsymbol{t}^H\boldsymbol{S}^{-1}\boldsymbol{y}_0}{(1+\boldsymbol{y}_0^H\boldsymbol{S}^{-1}\boldsymbol{y}_0)(\boldsymbol{t}^H\boldsymbol{S}^{-1}\boldsymbol{t})} \\ &= (K+1)T_{GLRT} = (K+1)\frac{\gamma}{1+\gamma}\end{aligned} \tag{18}$$

$$\begin{aligned} & \boldsymbol{y}_0^H \hat{\boldsymbol{R}}_0^{-1} \boldsymbol{y}_0 \\ &= (K+1)\boldsymbol{y}_0^H \boldsymbol{S}^{-1}\boldsymbol{y}_0 \left[1 - \left(1 + \boldsymbol{y}_0^H \boldsymbol{S}^{-1}\boldsymbol{y}_0\right)^{-1} \boldsymbol{y}_0^H \boldsymbol{S}^{-1}\boldsymbol{y}_0\right] \\ &= (K+1)\boldsymbol{y}_0^H \boldsymbol{S}^{-1}\boldsymbol{y}_0 \left(1 + \boldsymbol{y}_0^H \boldsymbol{S}^{-1}\boldsymbol{y}_0\right)^{-1} \\ &= (K+1)\left(1 - \frac{\varsigma}{\gamma+1}\right) \end{aligned} \tag{19}$$

$$\begin{aligned} T &= \widetilde{\boldsymbol{y}}_0^H \boldsymbol{P}_{\widetilde{\boldsymbol{t}}}^{\perp} \widetilde{\boldsymbol{y}}_0 \\ &= \boldsymbol{y}_0^H \boldsymbol{S}^{-1}\boldsymbol{y}_0 - \boldsymbol{y}_0^H \boldsymbol{S}^{-1}\boldsymbol{t}\left(\boldsymbol{t}^H \boldsymbol{S}^{-1}\boldsymbol{t}\right)^{-1} \boldsymbol{t}^H \boldsymbol{S}^{-1}\boldsymbol{y}_0 \\ &= \frac{1}{\varsigma} - 1 \end{aligned} \tag{20}$$

where $\gamma = \frac{\boldsymbol{y}_0^H \boldsymbol{S}^{-1}\boldsymbol{t}\boldsymbol{t}^H \boldsymbol{S}^{-1}\boldsymbol{y}_0}{\boldsymbol{t}^H \boldsymbol{S}^{-1}\boldsymbol{t}} / \left(1 + \boldsymbol{y}_0^H \boldsymbol{S}^{-1}\boldsymbol{y}_0 - \frac{\boldsymbol{y}_0^H \boldsymbol{S}^{-1}\boldsymbol{t}\boldsymbol{t}^H \boldsymbol{S}^{-1}\boldsymbol{y}_0}{\boldsymbol{t}^H \boldsymbol{S}^{-1}\boldsymbol{t}}\right)$, $\varsigma = 1/\left(1 + \boldsymbol{y}_0^H \boldsymbol{S}^{-1}\boldsymbol{y}_0 - \frac{\boldsymbol{y}_0^H \boldsymbol{S}^{-1}\boldsymbol{t}\boldsymbol{t}^H \boldsymbol{S}^{-1}\boldsymbol{y}_0}{\boldsymbol{t}^H \boldsymbol{S}^{-1}\boldsymbol{t}}\right)$. Since $\varsigma \sim C\beta_{K-N+2,N-1}$ and $\gamma \sim CF_{1,K-N+1}$ [21] are all independent of noise CM, the proposed detector is CFAR with respect to noise CM, where $C\beta$ and CF denote complex central beta distribution and complex central F-distribution, respectively.

4. Performance Assessment

Monte Carlo simulations are resorted to testing the matched and mismatched detection performance of the proposed detector. The threshold and detection probabilities are obtained by $100/P_{fa}$ and $1/P_{fa}$ independent trials. Unless otherwise specified, we set $P_{fa} = 10^{-4}$, $N = 16$, $\boldsymbol{t} = \left[1, e^{j2\pi f_d}, \ldots, e^{j2\pi(N-1)f_d}\right]$, $j = \sqrt{-1}$, $f_d = 0.08$. The noise CM is $\boldsymbol{R} = \boldsymbol{M} + \sigma^2 \boldsymbol{I}_N$, where $\boldsymbol{M}(i,j) = \exp\left[-2\pi^2 \sigma_f^2 (i-j)^2\right]$ denotes a Gaussian-shaped noise CM, $\sigma^2 \boldsymbol{I}_N$ denotes a white noise CM 10 dB weaker than the Gaussian-shaped noise, $\sigma_f = 0.05$. The signal-to-noise ratio (SNR) is

$$\text{SNR} = |\alpha|^2 \boldsymbol{t}^H \boldsymbol{R}^{-1} \boldsymbol{t} \tag{21}$$

4.1. CFAR Property Analysis

To analyze the CFAR property of the adaptive gradient detector, we set the correlation coefficient as: $\rho = \exp\left(-2\pi^2 \sigma_f^2\right)$. In Figure 1, we give the curves of P_{fa} versus ρ and σ. The curves show that P_{fa} stays almost the same for various ρ and σ. In other words, the false alarm probabilities of the proposed detectors are independent of noise CM. Thus, both the simulation results and theoretical analysis prove that the proposed adaptive gradient detector is CFAR with respect to noise CM.

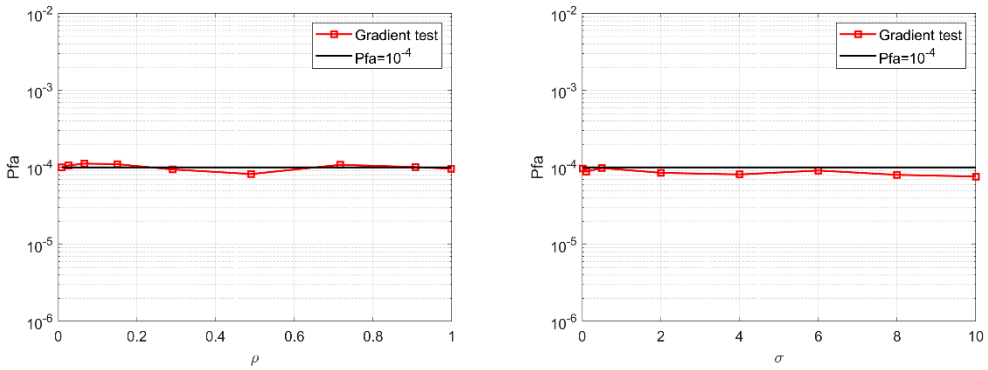

(**a**) (**b**)

Figure 1. CFAR property analysis for $N = 16$, $K = 2\,N$: (**a**) P_{fa} versus ρ of gradient test; (**b**) P_{fa} versus σ of gradient test.

4.2. Mismatched Detection Performance Analysis

Now, we test the mismatched detection performance of the proposed detector. We also give the performance of the robust parametric GLRT detector (PGLRT) proposed in [21] and the robust Rao and robust Wald detectors proposed in [24] for comparison. The detection performance of conventional AMF [2] and Kelly's GLRT [1] is also given. For clarity, we rewrote the test statistics of these detectors as

$$T_{GLRT} = \frac{\left|\boldsymbol{t}^H \boldsymbol{S}^{-1} \boldsymbol{y}_0\right|^2}{\left(1 + \boldsymbol{y}_0^H \boldsymbol{S}^{-1} \boldsymbol{y}_0\right)\left(\boldsymbol{t}^H \boldsymbol{S}^{-1} \boldsymbol{t}\right)} \tag{22}$$

$$T_{AMF} = \frac{\left|\boldsymbol{t}^H \boldsymbol{S}^{-1} \boldsymbol{y}_0\right|^2}{\boldsymbol{t}^H \boldsymbol{S}^{-1} \boldsymbol{t}} \tag{23}$$

$$T_{PGLRT} = \begin{cases} \frac{\left(1+\|\widetilde{\boldsymbol{y}}_0\|^2\right)\left(1-\frac{1}{\zeta_\varepsilon}\right)}{\left[(\zeta_\varepsilon - 1)\left\|\boldsymbol{P}_{\widetilde{\boldsymbol{t}}}^{\perp} \widetilde{\boldsymbol{y}}_0\right\|^2\right]^{\frac{1}{\zeta_\varepsilon}}}, \left\|\boldsymbol{P}_{\widetilde{\boldsymbol{t}}}^{\perp} \widetilde{\boldsymbol{y}}_0\right\|^2 > \frac{1}{\zeta_\varepsilon - 1} \\ \frac{1+\|\widetilde{\boldsymbol{y}}_0\|^2}{1+\left\|\boldsymbol{P}_{\widetilde{\boldsymbol{t}}}^{\perp} \widetilde{\boldsymbol{y}}_0\right\|^2}, \text{otherwise} \end{cases} \tag{24}$$

$$T_{Wald} = \frac{2(K+1)}{1+\hat{\delta}} T_{AMF} + \frac{NK\hat{\delta}^2}{(K+1)\left(1+\hat{\delta}\right)^2} \tag{25}$$

$$T_{Rao} = 2KT_{AMF} + \frac{(K+1)}{NK}\left[K\mathrm{tr}\left(\boldsymbol{S}^{-1}\boldsymbol{y}_0\boldsymbol{y}_0^H\right) - N\right]^2 \tag{26}$$

where $\zeta_\varepsilon = \frac{K+1}{N}(1+\varepsilon)$, $\varepsilon \geq 0$.

To analyze the robustness of the new gradient detector, we set the actual signal steering vector $\boldsymbol{t}_f = \left[1, e^{j2\pi f_{df}}, \ldots, e^{j2\pi(N-1)f_{df}}\right]$, where $f_{df} = f_d + \Delta/N$ denotes the Doppler frequency of the actual signal. When $\Delta = 0$, $\boldsymbol{t}_f$ and $\boldsymbol{t}$ are identical, that is, there is no signal mismatch. When the actual target steering vector $\boldsymbol{t}_f$ deviates from the nominal one $\boldsymbol{t}$, we define the mismatch angle as [13]

$$\cos^2\theta = \left|\boldsymbol{t}^H \boldsymbol{R}^{-1} \boldsymbol{t}_f\right|^2 / \left[\left(\boldsymbol{t}^H \boldsymbol{R}^{-1} \boldsymbol{t}\right)\left(\boldsymbol{t}_f^H \boldsymbol{R}^{-1} \boldsymbol{t}_f\right)\right] \tag{27}$$

The SNR becomes

$$\mathrm{SNR} = |\alpha|^2 \boldsymbol{t}_f^H \boldsymbol{R}^{-1} \boldsymbol{t}_f \tag{28}$$

Figures 2 and 3 plot detection probabilities versus SNR for $\Delta = 0.6$ ($\cos^2\theta = 0.16$) and $\Delta = 0.4$ ($\cos^2\theta = 0.46$). It can be seen that when the mismatch angle increases from $\cos^2\theta = 0.16$ to $\cos^2\theta = 0.46$, the detection probabilities of all the detectors increase. The Wald test suffers the most obvious performance degradation in signal mismatch cases. The proposed gradient test achieves comparable mismatched detection performance to the robust Rao test and outperforms other detectors for various K. When $\cos^2\theta = 0.46$, the gradient test achieves about 2 dB performance improvement compared with the robust PGLRT and AMF. When $\cos^2\theta = 0.16$, the gradient test achieves more than 1 dB and 6 dB performance improvement compared with the robust PGLRT and AMF, respectively.

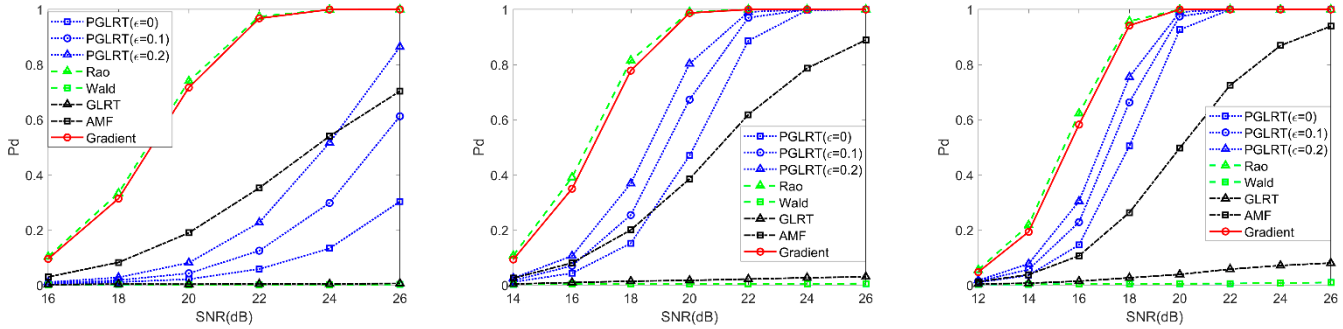

Figure 2. P_d versus SNR for $N = 16$, $\cos^2\theta = 0.16$: (**a**) $K = 24$; (**b**) $K = 32$; (**c**) $K = 40$.

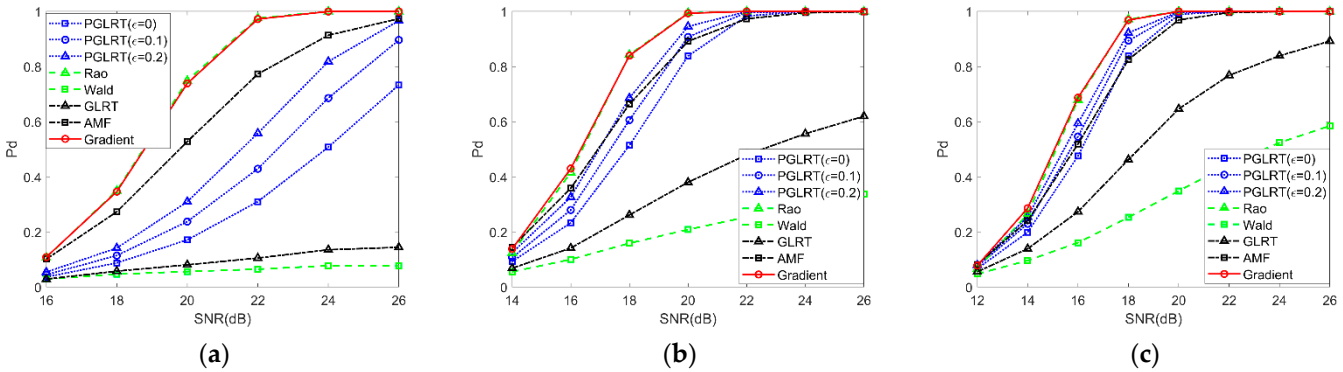

Figure 3. P_d versus SNR for $N = 16$, $\cos^2\theta = 0.46$: (**a**) $K = 24$; (**b**) $K = 32$; (**c**) $K = 40$.

In Figure 4, the probability of detection (P_d) as a function of $\cos^2\theta$ is plotted to analyze the gradient detector's mismatched detection performance when SNR $= 20$ dB and $K = 24,\ 32,\ 40$. In Figure 5, the contours of P_d of the detectors as a function of $\cos^2\theta$ and SNR when $K = 32$ is plotted. It can be seen that compared with the PGLRT, Wald, AMF, and Kelly's GLRT, the proposed gradient detector is more robust when the signal mismatch occurs. Compared with the robust Rao detector, the proposed gradient detector achieves better robustness when $\cos^2\theta > 0.46$.

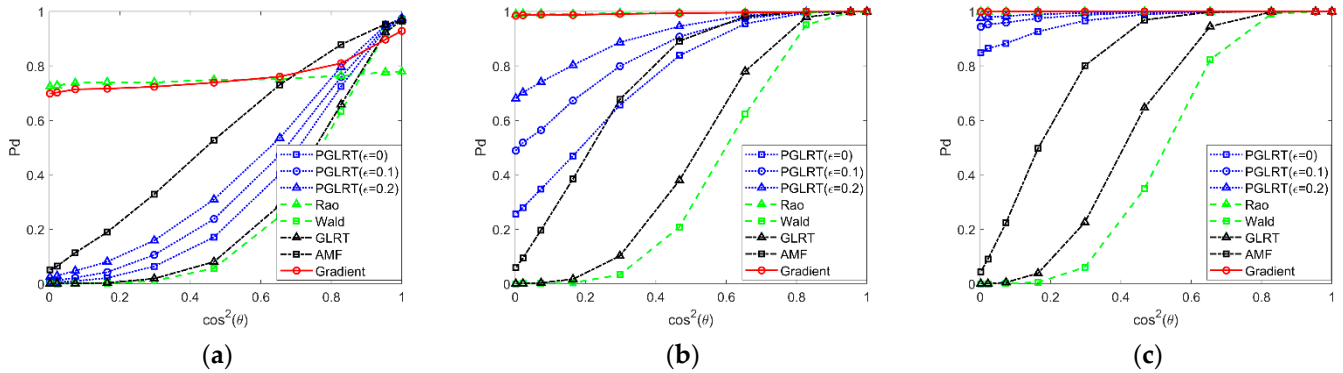

Figure 4. P_d versus $\cos^2\theta$ of the detectors for $N = 16$, SNR $= 20$ dB: (**a**) $K = 24$; (**b**) $K = 32$; (**c**) $K = 40$.

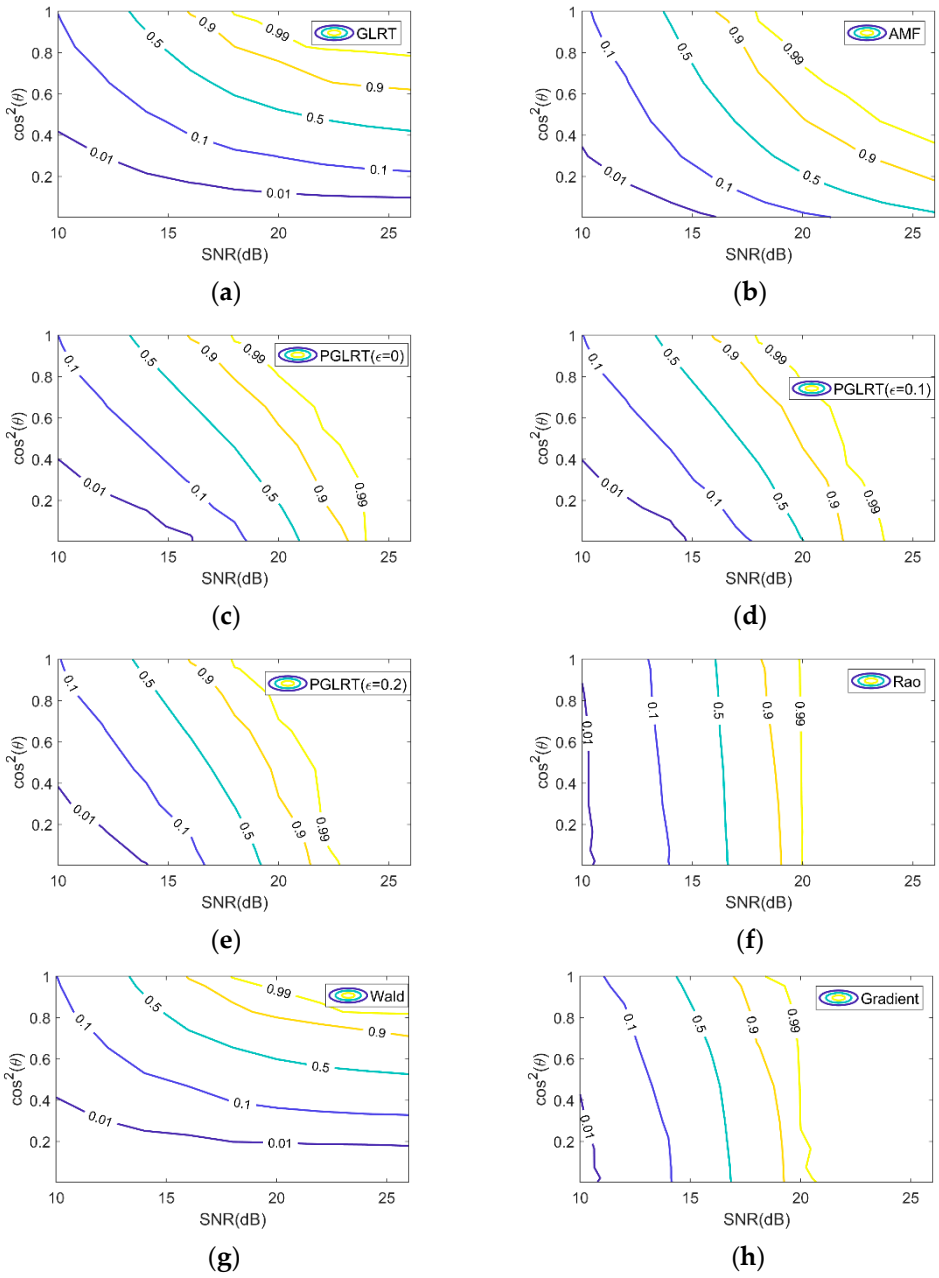

Figure 5. Contours of constant P_d of the detectors for $N = 16$, $K = 2$ N: (**a**) GLRT; (**b**) AMF; (**c**) PGLRT ($\varepsilon = 0$); (**d**) PGLRT ($\varepsilon = 0.1$); (**e**) PGLRT ($\varepsilon = 0.2$); (**f**) Rao test; (**g**) Wald test; (**h**) gradient test.

4.3. Matched Detection Performance Analysis

The detection probability curve versus SNR is shown in Figure 6 to test the adaptive gradient detector's matched detection performance. It can be seen that all the detectors achieve better-matched detection performance as the training data number increases. The Rao test performs the worst in the matched cases. Compared with the Rao test, the gradient detector shows increased matched detection performance. Compared with the PGLRT, AMF, Wald, and GLRT, the proposed gradient suffers certain matched detection performance loss. However, the matched detection performance loss is about 1 dB. Meanwhile, as shown in Figures 2–5, the proposed gradient detector still maintains suitable detection performance like the Rao test when a signal mismatch occurs, while other detectors suffer severe detection performance degradation. In conclusion, the gradient detector can achieve comparable robustness and improved matched detection performance compared to the Rao test. The gradient detector guarantees stronger robustness than PGLRT, AMF, Wald, and

GLRT in signal mismatch cases at the expense of a slight matched detection performance loss.

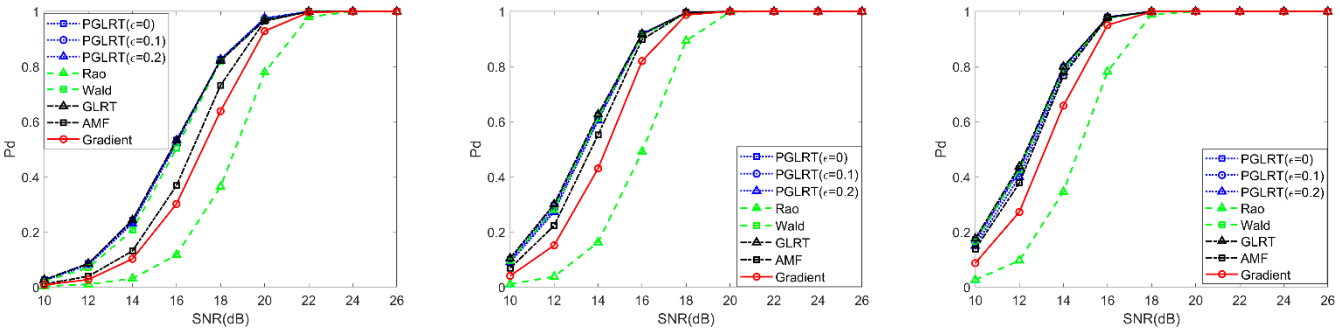

Figure 6. P_d versus SNR for $N = 16$, $\cos^2\theta = 1$: (**a**) $K = 24$; (**b**) $K = 32$; (**c**) $K = 40$.

4.4. Computation Complexity Analysis

To analyze the computation complexity of the proposed detector, we give the operation time of the eight detectors for $P_{fa} = 10^{-4}$, $\cos^2\theta = 1$, SNR = 10 dB and $K = 32$. To obtain the threshold and the detection probabilities, 10^4 independent Monte Carlo trials are conducted. Table 1 shows the mean operation time of 10 experiments. It can be seen that the AMF has the shortest operation time while the Wald test has the greatest computational burden.

Table 1. Computation complexity of the detectors.

Parameters	Operation Time(s)
PGLRT ($\varepsilon = 0.1, 0.2, 0.3$)	75.3228
Rao	72.6946
Wald	77.5186
GLRT	70.0076
AMF	68.3321
Gradient	76.2530

4.5. Experimental Results of IPIX Real Data

The VV polarimetric data of File 85 of the real datasets [26] collected using IPIX radar in Grimsby in 1998 is used to analyze the detection performance of the gradient detector. The real data have been preprocessed according to the steps in [27] to follow complex Gaussian distribution. The PDF curve of the measured data amplitude after preprocessing is shown in Figure 7. Due to the limited amount of measured data, we set $N = 8$, $K = 2N$, $P_{fa} = 10^{-2}$. Figure 8a shows the detection probability versus SNR in matched signal case. The performance loss of the gradient test compared with the PGLRT is less than 1 dB. Figure 8b plots the detection probability versus $\cos^2\theta$ for SNR = 20 dB. We can see that the gradient detector exhibits better robustness than PGLRT, AMF, Wald, and GLRT and comparable robustness to the Rao test.

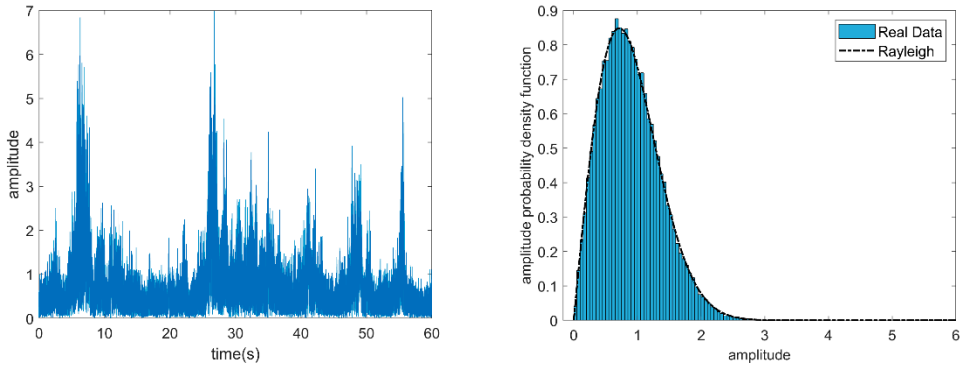

(**a**) (**b**)

Figure 7. Amplitude information of the real data: (**a**) amplitude of the real data; (**b**) PDF of the real data amplitude after preprocessing.

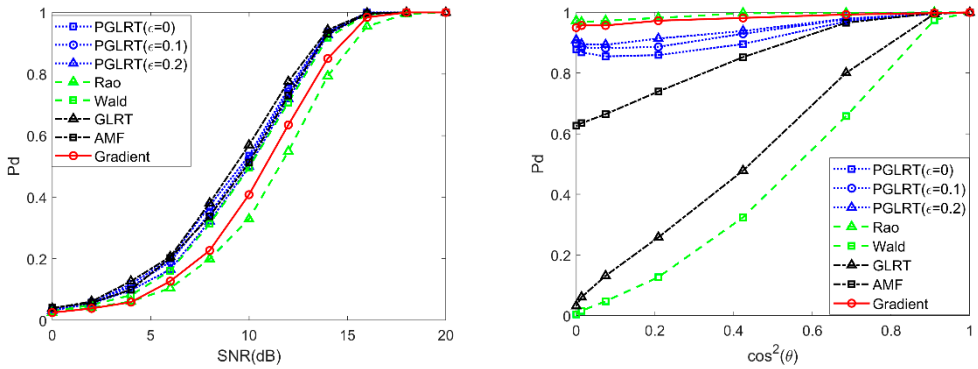

(**a**) (**b**)

Figure 8. Experimental results of IPIX real data for $N = 8$, $K = 16$: (**a**) P_d versus SNR for $\cos^2\theta = 1$; (**b**) P_d versus $\cos^2\theta$.

5. Conclusions

In this paper, the adaptive radar target detection problem in Gaussian noise has been considered. To increase the robustness, we have introduced a random perturbation under the alternative hypothesis. Under this assumption, the complex parameter gradient detector is proposed by treating complex parameters as a whole. The proposed gradient detector has been proven to have CFAR properties with respect to noise CM. The detection performance analysis based on simulated data and IPIX real data has highlighted that the gradient detector can achieve better robustness than Kelly's GLRT, AMF, and PGLRT and comparable robustness to the Rao test, which suffers severe matched detection performance loss in matched scenarios. A possible future track may be the investigation of designing robust detectors in non-Gaussian noise.

Author Contributions: The research presented in this manuscript was accomplished in collaboration with all of the authors. Conceptualization, Z.W.; methodology, Z.W. and J.L.; software, Z.W. and J.L.; validation, H.C. and W.Y.; formal analysis, H.C. and W.Y.; investigation, Z.W. and H.C.; resources, Z.W.; data curation, Z.W.; writing—original draft preparation, Z.W.; writing—review and editing, J.L. and H.C.; visualization, Z.W. and H.C.; supervision, Z.W. and H.C.; project administration, Z.W. and J.L.; funding acquisition, J.L. All authors have read and agreed to the published version of the manuscript.

Funding: This research was funded by the National Natural Science Foundation of China, grant number 61871469, Youth Innovation Promotion Association CAS, grant number CX2100060053, Anhui Provincial Natural Science Foundation, grant number 2208085J17.

Data Availability Statement: Not applicable.

Acknowledgments: The authors would like to thank the anonymous reviewers and the associate editor for their valuable comments.

Conflicts of Interest: The authors declare no conflict of interest.

References

1. Kelly, E.J. An adaptive detection algorithm. *IEEE Trans. Aerosp. Electron. Syst.* **1986**, *AES-22*, 115–127. [CrossRef]
2. Robey, F.C.; Fuhrmann, D.R.; Kelly, E.J.; Nitzberg, R. A CFAR adaptive matched filter detector. *IEEE Trans. Aerosp. Electron. Syst.* **1992**, *28*, 208–216. [CrossRef]
3. De Maio, A. A new derivation of the adaptive matched filter. *IEEE Signal Process. Lett.* **2004**, *11*, 792–793. [CrossRef]
4. Kraut, S.; Scharf, L.L.; McWhorter, L.T. Adaptive subspace detectors. *IEEE Trans. Signal Process.* **2001**, *49*, 1–16. [CrossRef]
5. De Maio, A. Rao test for adaptive detection in Gaussian interference with unknown covariance matrix. *IEEE Trans. Signal Process.* **2007**, *55*, 3577–3584. [CrossRef]
6. Liu, X.; Du, L.; Xu, S. GLRT-Based coherent detection in sub-Gaussian symmetric alpha-stable clutter. *IEEE Geosci. Remote Sens. Lett.* **2022**, *19*, 8015405. [CrossRef]
7. Song, C.; Wang, B.; Xiang, M.; Wang, Z.; Xu, W.; Sun, X. A novel post-doppler parametric adaptive matched filter for airborne multichannel Radar. *Remote Sens.* **2020**, *12*, 4017. [CrossRef]
8. Chen, X.; Cheng, Y.; Wu, H.; Wang, H. Heterogeneous clutter suppression for airborne radar STAP based on matrix manifolds. *Remote Sens.* **2021**, *13*, 3195. [CrossRef]
9. Wang, Z.; Liu, J.; Li, Y.; Chen, H.; Peng, M. Adaptive Subspace Signal Detection in Structured Interference Plus Compound Gaussian Sea Clutter. *Remote Sens.* **2022**, *14*, 2274. [CrossRef]
10. Xue, J.; Xu, S.; Liu, J.; Pan, M.; Fang, J. Bayesian detection for radar targets in compound-Gaussian Sea clutter. *IEEE Geosci. Remote Sens. Lett.* **2022**, *19*, 4020805. [CrossRef]
11. Wang, Z.; Li, G.; Chen, H. Adaptive persymmetric subspace detectors in the partially homogeneous environment. *IEEE Trans. Signal Process.* **2020**, *68*, 5178–5187. [CrossRef]
12. De Maio, A.; Farina, A.; Gerlach, K. Adaptive detection of range spread targets with orthogonal rejection. *IEEE Trans. Aerosp. Electron. Syst.* **2007**, *43*, 738–752. [CrossRef]
13. Pulsone, N.B.; Rader, C.M. Adaptive beamformer orthogonal rejection test. *IEEE Trans. Signal Process.* **2001**, *49*, 521–529. [CrossRef]
14. Bandiera, F.; Besson, O.; Ricci, G. An ABORT-like detector with improved mismatched signals rejection capabilities. *IEEE Trans. Signal Process.* **2008**, *56*, 14–25. [CrossRef]
15. Besson, O. Detection in the presence of surprise or undernulled interference. *IEEE Signal Process. Lett.* **2007**, *14*, 352–354. [CrossRef]
16. Orlando, D.; Ricci, G. A Rao test with enhanced selectivity properties in homogeneous scenarios. *IEEE Trans. Signal Process.* **2010**, *58*, 5385–5390. [CrossRef]
17. De Maio, A. Robust adaptive radar detection in the presence of steering vector mismatches. *IEEE Trans. Aerosp. Electron. Syst.* **2005**, *41*, 1322–1337. [CrossRef]
18. Liu, J.; Li, J. Robust detection in MIMO radar with steering vector mismatches. *IEEE Trans. Signal Process.* **2019**, *67*, 5270–5280. [CrossRef]
19. Besson, O. Adaptive detection with bounded steering vectors mismatch angle. *IEEE Trans. Signal Process.* **2007**, *55*, 1560–1564. [CrossRef]
20. Shen, L.; Liu, Z.; Xu, Y.; Bai, Y.; Zhao, T. Robust polarimetric adaptive detector against target steering matrix mismatch. *IEEE Trans. Aerosp. Electron. Syst.* **2020**, *56*, 442–455. [CrossRef]
21. Coluccia, A.; Ricci, G.; Besson, O. Design of robust radar detectors through random perturbation of the target signature. *IEEE Trans. Signal Process.* **2019**, *67*, 5118–5129. [CrossRef]
22. Kay, S.; Zhu, Z. The complex parameter Rao test. *IEEE Trans. Signal Process.* **2016**, *64*, 6580–6588. [CrossRef]
23. Sun, M.; Liu, W.; Liu, J.; Hao, C. Complex parameter Rao, Wald, gradient, and Durbin tests for multichannel signal detection. *IEEE Trans. Signal Process.* **2022**, *70*, 117–131. [CrossRef]
24. Sun, S.; Liu, J.; Liu, W.; Jian, T. Robust detection of distributed targets based on Rao test and Wald test. *Signal Process.* **2021**, *180*, 107801. [CrossRef]
25. Kelly, E.J.; Forsythe, K. *Adaptive Detection and Parameter Estimation for Multidimensional Signal Models*; Technical Report 848; Lincoln Laboratory: Lexington, KY, USA, 1989.
26. The McMaster IPIX Radar Sea Clutter Database. Available online: http://soma.ece.mcmaster.ca/ipix/ (accessed on 1 June 2019).
27. Tang, P.; Wang, Y.-L.; Liu, W.; Du, Q.; Wu, C.; Chen, W. A tunable detector for distributed target detection in the situation of signal mismatch. *IEEE Signal Process. Lett.* **2020**, *27*, 151–155. [CrossRef]